Journal of Power Sources 251 (2014) 411–416

Contents lists available at ScienceDirect

Journal of Power Sources

journal homepage: www.elsevier.com/locate/jpowsour

Hydrothermal synthesis of $LiMn_2O_4$ onto carbon fiber paper current collector for binder free lithium-ion battery positive electrodes

Gordon Henry Waller, Samson Yuxiu Lai, Ben Harris Rainwater, Meilin Liu*

School of Materials Science and Engineering, Georgia Institute of Technology, Atlanta, GA 30332-0245, USA

HIGHLIGHTS

- Direct growth of crystalline $LiMn_2O_4$ on carbon fibers.
- Binder, tape casting, and metal foil free electrodes for lithium ion batteries.
- Low temperature synthesis using hydrothermal precipitation.
- Half cell testing shows high capacity at moderate rates.

ARTICLE INFO

Article history:
Received 3 September 2013
Received in revised form
4 November 2013
Accepted 21 November 2013
Available online 3 December 2013

Keywords:
Spinel
Lithium ion battery
Positive electrode
Carbon fiber
Hydrothermal

ABSTRACT

Concerns over the safety and high cost of lithium ion batteries, especially those containing cobalt-based active materials, limit their use to applications where energy density requirements cannot be met by any other materials. Manganese-spinel based positive electrode materials represent a promising candidate for lithium ion batteries because of their lower cost, lower toxicity, and greater resistance to thermal runaway than cobalt-based active materials. Although $LiMn_2O_4$ has a well-known issue of capacity fading, investigations into nanostructured composites composed of surface modified spinel phases have demonstrated outstanding performance, suggesting that $LiMn_2O_4$ has potential to be a viable positive electrode for safe, inexpensive, high power, and long lifetime lithium-ion batteries. Here we report a low-temperature hydrothermal process for growth of conformal coatings of highly crystalline $LiMn_2O_4$ directly onto a carbon fiber current collector, completely eliminating the process steps and materials associated with the conventional tape casting approach (binders, solvents, and metal foils). The prepared electrodes tested at a rate of 1 C showed an initial discharge capacity of 125 mAh g^{-1} and an average energy efficiency of 92.4% over 100 cycles.

1. Introduction

When compared with $LiCoO_2$ (the early lithium ion battery positive electrode), $LiMn_2O_4$ has safety and cost advantages with comparable energy density. $LiMn_2O_4$ is considered to be a safer material than $LiCoO_2$ due to its superior thermal stability and because the Co salts used to synthesize $LiCoO_2$ positive electrode materials are toxic [1,2]. Manganese is more naturally abundant than cobalt and, as a result, $LiMn_2O_4$ electrodes would be cheaper to produce. While $LiCoO_2$ has a much higher theoretical capacity (274 mAh g^{-1} compared to 148 mAh g^{-1} for $LiMn_2O_4$), $LiCoO_2$ is limited to extracting about 0.55 Li per formula unit before detrimental structural changes occur [3]. Because of the extraction limit of $LiCoO_2$ and the similar half cell potentials of the oxides, their energy densities are comparable. Unfortunately $LiMn_2O_4$ experiences accelerated capacity fading compared to $LiCoO_2$, especially at elevated temperatures, which has been reported to be caused by dissolution of Mn into the electrolyte by HF impurities in $LiPF_6$-containing electrolytes [4]. Several approaches have been effective at limiting the capacity loss for cycled $LiMn_2O_4$, including changing the electrolyte salt [5] or introducing protective layers [5–7].

Today, state-of-the-art positive electrodes are mixed cation layered oxides isostructural with $LiCoO_2$. These materials allow closer to 1 lithium extraction per formula unit, greatly enhancing energy densities [8–10]. While commercial application of $LiMn_2O_4$ has been limited, research into nanostructured $LiMn_2O_4$ has shown that certain morphologies produce exceptional rate capabilities [11,12], enhanced capacity retention (even with fluorine-containing electrolyte) [13], and the ability to cycle below the 3 V vs. Li/Li^+ potential region in which a Jahn–Teller distortion normally causes

* Corresponding author.
E-mail address: meilin.liu@mse.gatech.edu (M. Liu).

0378-7753/$ – see front matter © 2013 Elsevier B.V. All rights reserved.
http://dx.doi.org/10.1016/j.jpowsour.2013.11.081

additional capacity loss [14]. These considerations provide impetus towards re-evaluating $LiMn_2O_4$ as a commercial viability.

One branch of research into nanostructured $LiMn_2O_4$ has introduced an interesting dynamic to this re-evaluation. Namely, crystalline $LiMn_2O_4$ can be produced at very low temperatures via hydrothermal synthesis compared to solid-state calcinations routes usually occurring above 500 °C. One approach uses pre-formed Mn-oxide (e.g. MnO_2) starting material as a template and reacts this with a solution of lithium salts in a hydrothermal autoclave to produce $LiMn_2O_4$ [15,16]. These reactions have relatively high hydrothermal temperatures (≥200 °C) and long dwell times, requiring up to several days for a complete conversion. Another approach uses potassium permanganate ($KMnO_4$) in which manganese exists in the water soluble +7 oxidation state and can be readily reduced to form insoluble Mn-oxides. An aqueous solution of $KMnO_4$, LiOH, and a reducing agent can be used to obtain nanocrystalline $LiMn_2O_4$ at temperatures below 200 °C in a matter of hours [17]. An interesting variation of this approach incorporates carbon into the hydrothermal solution. Carbon itself can serve as a reducing agent for $KMnO_4$ to form MnO_2 nanostructured composites [18,19]. Composites formed in this way show enhanced rate capabilities [20], especially when using carbon nanotubes [20–22].

Regardless of the fabrication methods, powders used as active materials in lithium ion batteries are typically formed into electrodes using a ubiquitous tape casting process, which introduces certain limitations to electrode design. The cast tape consists of slurry of active material and binder in a solvent. A common solvent used for this process is *N*-methyl-2-pyrrolidone (NMP), which is toxic and expensive [23]. For positive electrodes, a conductive dilutant, usually carbon, is added to raise the electrical conductivity of the composite electrode and greater amounts of carbon must be added to the slurry for higher power operation [24]. Tradeoffs between electrode energy density and rate capability, which are influenced by electrode thickness, weight percentage of inactive materials, and porosity, are necessarily inversely related [25].

Porous current collectors have also been applied to solve some of the issues inherent to tape-cast electrodes. Such structures can be made much thicker than tape-cast electrodes while maintaining ionic and electronic conduction pathways. Foams of metal and carbon have been demonstrated extensively for their application as porous current collectors in electrochemical devices [26–29]. Whitehead and Schreiber reported that carbon current collectors have good electrochemical stability but are limited by their electrical conductivity [30]. However, the work of Dudney et al. has demonstrated that networks of carbon fibers infiltrated with a slurry containing pre-formed $LiFePO_4$ powder are capable of high cycling efficiency and high power outputs [31,32]. Work by our group and others have focused on producing porous electrodes for electrochemical devices by growing oxide active materials directly onto carbon fiber paper (CFP) using hydrothermal synthesis [33–35]. In this report, a single-step assembly of $LiMn_2O_4$ nanocrystals directly on sheets of carbon fiber paper at low temperature is described. This approach removes the need for tape casting and the associated binders and solvents and greatly simplifies electrode assembly.

2. Experimental section

2.1. Preparation of $LiMn_2O_4$ on CFP electrode

The carbon fiber paper (CFP) used in this study was provided by Engineered Fibers Technology, LLC and has a network of interconnecting fibers with diameters averaging 8–10 μm with a total thickness of about 200 μm. An SEM image of the uncoated carbon fiber paper is shown in Fig. S1. Pieces of carbon fiber paper with dimensions of 2.5 cm × 5 cm were first activated using a heat treatment at 300 °C for 3 h. This heat treatment made the CFP more hydrophilic, enhancing the capillary action of the CFP and improving coating homogeneity during the subsequent processing. The heat-treated CFP was placed into a 200 mL Teflon-lined stainless-steel autoclave and oriented upright using a notched Teflon support. A solution of 20 mM NH_4Cl, 20 mM $KMnO_4$, and 50 mM LiOH in distilled water was prepared by magnetic stirring at room temperature for 20 min until all the reagents were dissolved. The solution had a dark purple color that did not change with extended stirring, implying no immediate reduction of the permanganate ions. The solution was added into the autoclave, covering the CFP with a fill factor of 80%, then sealed and allowed to sit at room temperature for a period of 3 h for the solution to soak into the CFP. After the soaking period, the autoclave was placed in a furnace and heated to 100 °C at a rate of 3 °C min^{-1} and held at that temperature for 12 h. Following this, the furnace was heated at 3 °C min^{-1} to 140 °C for 24 h and then cooled at the same rate. After the hydrothermal procedure the solution was clear and the CFP appeared to be covered in a black coating (CFP/LMO). The CFP/LMO was rinsed several times with distilled water to remove residual salts from the hydrothermal procedure. As a comparison to the commercially available CFP, we also developed a carbon fiber net with smaller diameter carbon fibers using electrospinning. The electrospinning parameters used are described in Supporting information, and an uncoated net of electrospun fibers is shown in Fig. S2. These fibers have a wider range of diameters than the commercially available CFP but most fibers fall between 0.75 and 2.5 μm.

2.2. Physical characterization

Pieces of the larger CFP/LMO sample were cut out and prepared for X-ray Diffraction (XRD) and Scanning Electron Microscope (SEM) analysis. A PANalytical X'Pert PRO Alpha-1 with Cu K-α1 source was used for the X-ray diffraction experiments. The SEM used was a LEO 1530 thermally-assisted field emission scanning electron microscope. No additional conductive coating was needed for the SEM analysis. To determine the mass loading of the CFP/LMO, pieces of bare CFP heat treated as per the pre-hydrothermal routine were weighed with a lab balance after vacuum drying inside an argon filled glovebox, with pieces of CFP/LMO weighed in a similar manner. Thermogravimetric analysis was performed to confirm the measurements made with the lab balance using a TA Instruments Q600 SDT with air (Airgas, Ultra Zero purity) as the purge gas. After taring the alumina pans, samples of 10 mg or less were loaded and allowed to rest at room temperature for at least 1 h under 100 mL min^{-1} of purge gas until the mass loss due to suspected water evaporation stabilized, as observed in Fig. S3. Once the sample mass stabilized, the sample was heated at 10 °C min^{-1} to 900 °C to oxidize the CFP. The remaining mass is then presumed to be the oxide coating.

2.3. Electrochemical measurements

Using a circular punch, electrodes with a superficial area of approximately 1 cm^2 were cut from the larger $LiMn_2O_4$-coated CFP piece. These electrodes were placed in a vacuum drying oven at 100 °C overnight and then immediately placed into an argon filled glovebox. The electrodes were assembled into half-cells using glass fiber separators (Whatman GF/D) soaked with 1 M $LiPF_6$ in 1:1 ethylene carbonate/dimethyl carbonate electrolyte (Novolyte). A piece of Li metal with an area of 1.26 cm^2 was used as both the counter and pseudo-reference electrode. All electrochemical measurements were made using an Arbin BT-2000 battery tester. For

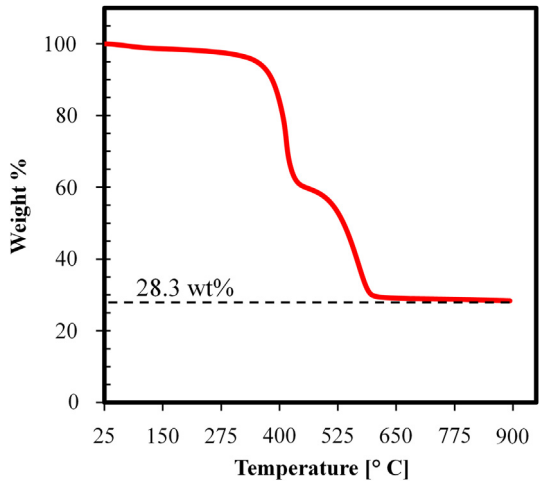

Fig. 1. Thermogravimetric analysis of $LiMn_2O_4$ on CFP used to determine the oxide mass loading. Mass loss is associated with oxidation of the carbon fiber paper by heating in air.

cycling measurements, current was fixed to a desired C rate using the mass of the active material and the cell was charged or discharged until the cell potential reached the desired cutoff. The charging cutoff potential was set at 4.5 V vs. Li/Li^+ and the discharge value was set at 3.0 V vs. Li/Li^+. Charging steps also included a constant potential "trickle charge" time period of 1 h during which time the current decayed. No equivalent constant potential was used during discharge steps, however both charge and discharge steps included a rest period of 1 h at open circuit conditions once the cutoff voltage was reached. Neither the CFP or electrospun carbon fiber based electrodes showed any signs of mechanical degradation after electrochemical testing, which used a "Swagelok" cell configuration that applied pressure to the electrodes with a stainless steel spring. Digital images of the both electrode types after disassembly are shown in Fig. S4.

3. Results and discussion

After vacuum drying, the average mass of several CFP/LMO electrodes measured in an argon filled glovebox was 14 mg cm^{-2}, while the bare CFP pieces had an average mass of 10 mg cm^{-2}. From these measurements the amount of active material was found to be about 4.0 mg cm^{-2}, or 28 wt%. Individual electrodes weighed prior to half cell assembly had a mass deviation within ±0.1 mg. These values were confirmed with thermogravimetric analysis (Fig. 1), which reported a mass loading of 28.3 wt%. During assembly, it was observed that the excellent wetting that existed in the bare heat treated CFP is retained in the coated CFP/LMO electrodes. Drops of electrolyte added to the electrode were quickly wicked into the electrode. The rate at which electrolyte can infiltrate a tape cast electrode has been reported as the limiting factor in cell assembly speeds [24].

At hydrothermal temperatures of 100 °C, a conformal coating with a flower-like morphology is observed using SEM (Fig. 2a–c). The "flowers" have "petals" a few tens of nanometers thick. Coatings produced at 140 °C and above are coated with a layer of discrete multi-faceted crystallites, ranging in size from 50 to 500 nm, as shown in Fig. 2d–f. These coatings have a thickness of about 2 μm, with nodules protruding beyond this in some parts which are also observed in the flower-like coatings. Coatings produced at 100 °C were found to be mostly amorphous using XRD (Fig. 3), with only a few shallow peaks that seem to be consistent with the potassium stabilized MnO_2-birnessite phase observed by others using the potassium permanganate hydrothermal route to synthesize $LiMn_2O_4$ [17]. For a reaction temperature of 140 °C, the coatings were found to be phase-pure, highly crystalline $LiMn_2O_4$. At a temperature of 160 °C, an impurity phase of Mn_3O_4 is also observed and the diffraction peaks for $LiMn_2O_4$ show decreased intensity relative to the CFP background diffraction. Thus, it seems probable that the $LiMn_2O_4$ crystallites nucleate directly from the flower-like coatings first formed at lower temperatures before converting to the spinel $LiMn_2O_4$ at 140 °C. The XRD results for coatings produced at temperatures of 100 °C, 140 °C, and 160 °C, along with the data from the bare CFP, are shown in Fig. 3. We found that by performing the hydrothermal treatment in two stages, first at 100 °C to favor the formation of the birnessite structured, flower-like coating and then heating to 140 °C and holding at this temperature for conversion to the spinel structure, the $LiMn_2O_4$ coatings had greater uniformity throughout the CFP and increased mass loading. All of the data reported for coatings fabricated at 140 °C were created in this way. A comparison between the XRD results for samples containing hydrothermal $LiMn_2O_4$ on CFP and commercial

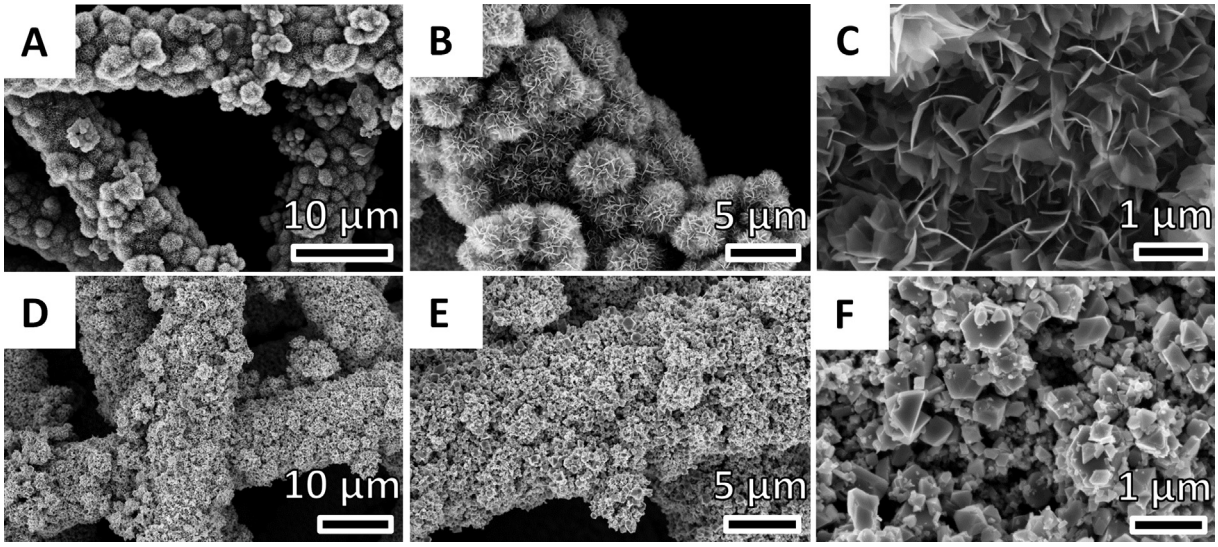

Fig. 2. Scanning electron microscope images of carbon fiber papers coated using hydrothermal synthesis at 100 °C (a–c) and 140 °C (d–f). The samples in images d-f were produced using the two step heating approach described in the Results and Discussion section.

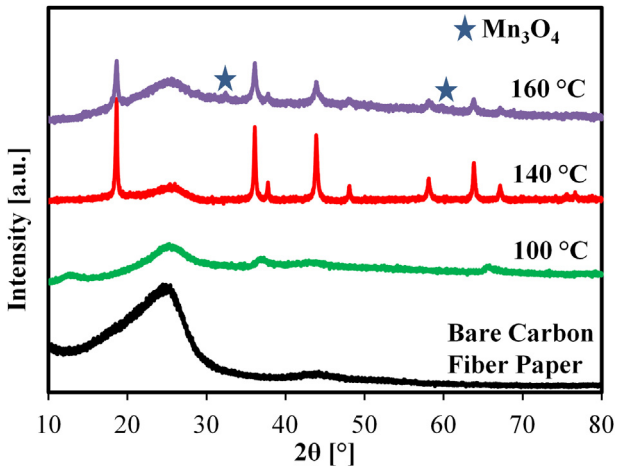

Fig. 3. X-ray diffraction data from bare CFP and samples of coated CFP using the described hydrothermal synthesis parameters.

$LiMn_2O_4$ powders is shown in Fig. S5. For the coatings produced at a maximum temperature of 140 °C using the two-step approach, analysis of the (111) diffraction peak using Bragg's Law yields a calculated lattice parameter for a cubic unit cell of 8.245 Å, close to the reference value (ICDD 00-035-0782) of 8.2476 Å. From this we can infer that the stoichiometry of the as prepared sample is close to that of $LiMn_2O_4$, with lithium atoms mostly occupying tetrahedral sites in the oxygen FCC lattice [17].

Cyclic voltammetry measurements of freshly prepared half cells (Li metal/1 M $LiPF_6$ in 1:1 EC:DMC/$LiMn_2O_4$ on CFP) reveal two sharp, individually resolvable redox peaks with current maximums around 4.04 and 4.16 V vs. Li/Li^+ during charge and 4.10 and 3.98 V vs. Li/Li^+ during discharge, as shown in Fig. 4. These values are close to what have been reported for $LiMn_2O_4$ produced using high temperature calcinations to ensure excellent crystallinity [11,36]. Furthermore, the redox potentials observed using cyclic voltammetry do not shift substantially after 100 cycles at a 1 C rate (Fig. S6). At a relatively low sweep rate of 50 μV s^{-1}, the background current observed far from the redox peaks is large, which is caused by the large surface area and the associated double-layer capacitance of the oxide coated carbon fiber electrodes. This observation is consistent with our previous work; however, the contribution to the total charge storage capability of the electrode from double-layer capacitance is not clear [33,34]. Galvanostatic charge and discharge cycling was used to determine specific capacity and rate capability of the electrodes. All charge and discharge measurements began with a formation procedure consisting of five cycles at a C/25 rate (1 C is 148 mA g^{-1}) between the potentials of 4.5 and 3.0 V vs. Li/Li^+. The discharge capacity averaged over several samples at the end of the formation procedure is 146 mAh g^{-1}.

At low discharge rates, the ohmic overpotential observed is small and the discharge potentials are in agreement to those observed with cyclic voltammetry. At rates up to 1 C, the discharge potential plateau is above 3.9 V vs. Li/Li^+ with an initial discharge capacity after the formation procedure of 125 mAh g^{-1}. A comparison between the discharge voltage profiles for various rates after the formation procedure is shown in Fig. 5. At a rate of 5 C, the discharge potential is noticeably depressed, leading to a decrease in available discharge capacity to 98.8 mAh g^{-1} after the formation procedure. Fig. 6a shows the discharge capacity at various rates for 50 cycles. The first five cycles for each electrode show the discharge capacity for the formation procedure and are included as a baseline for electrodes tested at different rates. All reported rates are for both charge and discharge, though each charge step was followed by a potentiostatic trickle charge in which the cell was held at 4.5 V vs. Li/Li^+ for 1 h. The decay in specific current during the trickle charge time period is illustrated in Fig. S6 following a charge step at a 1 C rate (148 mA g^{-1}), which is in effect for the first portion of the graph between 4.25 and 4.5 V vs. Li/Li^+. This current decay is consistent with previously reported studies on the electrochemical stability of carbon fibers, namely that carbon oxidation or electrolyte degradation (for a $LiPF_6$ salt in EC/DMC solvent electrolyte) at potentials up to 4.5 V vs. Li/Li^+ is not significant [30,37]. The percentage of total charge capacity obtained during the galvanostatic portion compared to the total charge capacity (galvanostatic and potentiostatic) is shown in Table S1. At the end of 50 cycles, the electrodes cycled at C/5, 1 C, and 5 C retain 89.7, 93.2, and 90.4% of their initial discharge capacities, respectively. In Fig. 6b, the charge and discharge capacities for 100 cycles at a 1 C rate are shown and

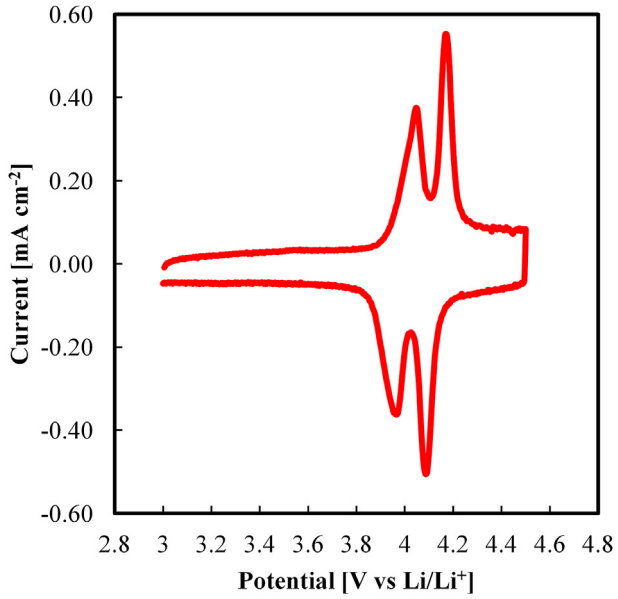

Fig. 4. Cyclic voltammetry for a freshly assembled $LiMn_2O_4$ on CFP half cell at a sweep rate of 50 μV s^{-1}.

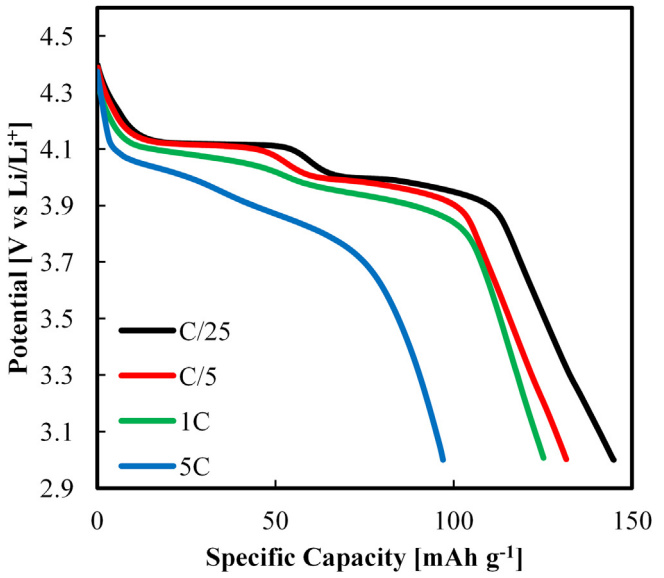

Fig. 5. Potential profiles for CFP/LMO electrodes discharged at various constant current values. C/25 discharge was for last cycle of the formation procedure, all other values are for the second discharge at the specified rate following the formation procedure.

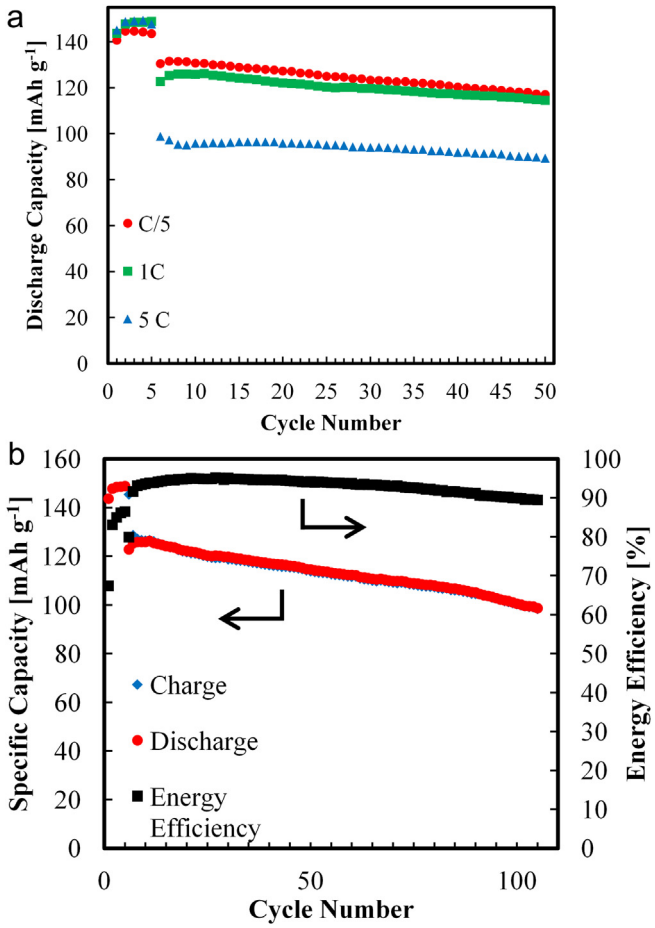

Fig. 6. a) Discharge capacities for CFP/LMO electrodes cycled at various rates (quoted rates are for charge and discharge). b) Charge and discharge capacity for CFP/LMO electrode cycled at 1 C rate. Energy efficiency is the ratio of the charge and discharge energy in watt-hours.

plotted along with the energy efficiency (watt-hours discharged divided by watt-hours charged), which has an average value of 92.4%.

To further investigate the use of carbon fibers as pre-formed current collectors for porous electrodes, we applied the same coating technique used on CFP to a network of smaller carbon fibers created via electrospinning. After coating, the electrospun fibers resemble the coated CFP. SEM images of the coated electrospun fibers are shown in Fig. 7. The thickness of the coated electrospun fiber electrode is close to that of the commercial fibers at 210 μm vs. 200 μm for the CFP electrode. As anticipated, reducing the fiber diameter dramatically increases the oxide mass loading. Mass

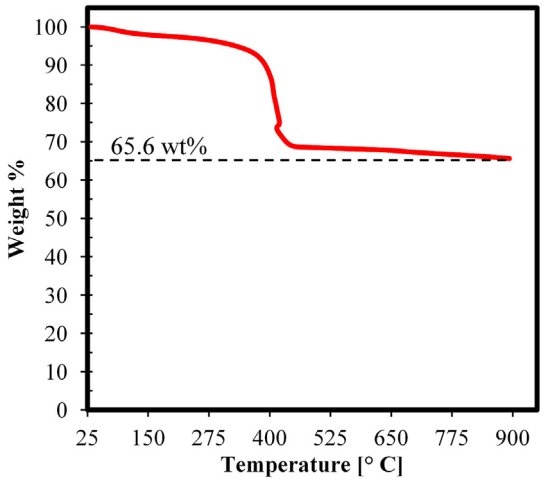

Fig. 8. Thermogravimetric analysis of $LiMn_2O_4$ on electrospun carbon fibers shows increase mass content of oxide relative to carbon fiber current collector.

measurements using TGA show that the electrospun fibers have mass loadings in excess of 65 wt%, shown in Fig. 8. This increase in mass loading also leads to a small increase in volumetric capacity, shown in Table S2. Unfortunately, a drop in electrochemical performance similar to the coated CFP was observed at a rate of 5 C. An identical plot to Fig. 5 for coated CFP is shown in Fig. S8 for the coated electrospun fibers.

At this point, the factors limiting rate capability are still not clear. In the case of the electrospun carbon fiber current collector, the total thickness of the oxide coating is about 500 nm as determined by the change in apparent fiber diameter between coated and un-coated fibers, while the crystallites within the coating range in size from 50 nm to 250 nm. This should allow sufficiently fast ionic transport in the electrodes compared to conventional active material particulates with diameters of tens of microns, leading us to believe that the rate limiting factor is likely the electronic resistance of the electrodes. Despite the relatively high carbon content of our electrodes, some of the active materials may be partially isolated from the current collector. Furthermore, the Swagelok cell configuration used for testing depends on the in-plane electron transport of the electrode, which may be increased by the contact resistance between several layers of oxide coated carbon fibers, whereas the conductivity within an individual carbon fiber is assumed to be suitably high. Thus, while it is reasonable to anticipate further improvements in mass loading using electrospun fibers of various diameters and geometries (e.g. hollow fibers), careful design of electrode architecture (e.g. the carbon fiber mat) is needed to maximize electrochemical performance.

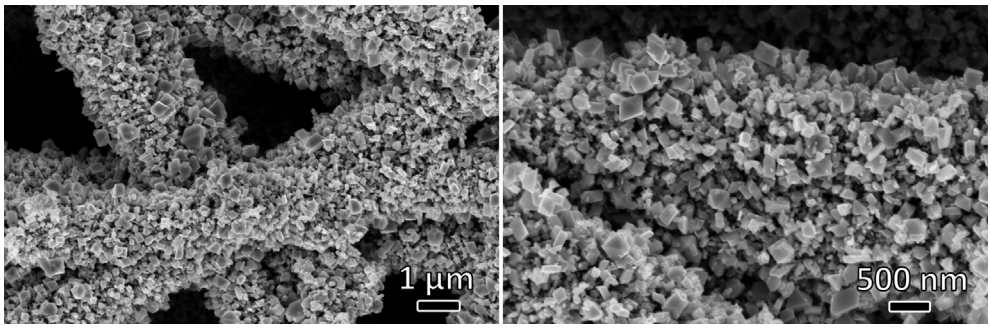

Fig. 7. SEM images of electrospun carbon fibers coated with $LiMn_2O_4$ using identical parameters to those described for coating commercially available CFP.

4. Conclusion

In this report, carbon fiber paper scaffolds coated with $LiMn_2O_4$ in a low temperature hydrothermal synthesis were used to produce positive electrodes for lithium ion batteries. The initial discharge capacity at a 1 C rate was 125 mAh g^{-1} with an average energy efficiency of 92.4% over 100 cycles. The specific capacity and rate capability reported here for $LiMn_2O_4$ on carbon fiber paper electrodes is comparable to other work in the area of low temperature hydrothermal synthesis [17] and carbon supported $LiMn_2O_4$ powders [20], while another binder free approach showed lower capacities at similar rates [38]. At approximately 28 wt% $LiMn_2O_4$, the electrodes created using commercial carbon fiber paper have significantly less active material than conventional tape-cast electrodes which usually report 80–90 wt% active material in composite electrode. By using smaller diameter electrospun fibers, mass loadings of over 65 wt% were obtained. Finally, when considering the total mass of a tape cast electrode, the mass of the foil current collector should be included. With the contribution from the current collector included, one report estimates the weight percentage of active material in a positive electrode for a high power cell is only 72 wt% of the total electrode mass [24]. Still, the high rate electrochemical performance for these electrodes should be further improved. Future work will focus on optimizing the diameter and morphology of carbon fibers used to further increase the oxide mass loading, potentially beyond the range possible for tape cast electrodes. Additionally, the novel electrode architecture reported here could enable simultaneous application of coatings to a complete electrode. Such coatings will be aimed at enhancing the rate capability, for example by using a thin layer of carbon, and improving capacity retention for $LiMn_2O_4$ electrodes following the methods reported elsewhere [6,39]. The advantage of our approach is that complete electrodes are formed in one step without the need to collect hydrothermal precipitates, thus subtracting the processing steps and costs associated with the binders and solvents used for tape casting. It can be imagined that any variety of carbon current collectors could be pre-formed with desired geometries, for example carbon foams, and then directly coated with active materials, which could yield enhanced performance compared to tape cast electrodes [26,40].

Acknowledgments

This material is based upon work supported as part of the HeteroFoaM Center, an Energy Frontier Research Center funded by the U.S. Department of Energy (DOE), Office of Science, Office of Basic Energy Sciences (BES) under Award Number DESC0001061. The authors acknowledge Engineered Fibers Technology, LLC of Wilmington, DE for samples of carbon fiber paper and consultation on their product.

Appendix A. Supplementary data

Supplementary data related to this article can be found at http://dx.doi.org/10.1016/j.jpowsour.2013.11.081.

References

[1] D.D. MacNeil, T.D. Hatchard, J.R. Dahn, J. Electrochem. Soc. 148 (2001) A663–A667.
[2] N.S. Choi, Z.H. Chen, S.A. Freunberger, X.L. Ji, Y.K. Sun, K. Amine, G. Yushin, L.F. Nazar, J. Cho, P.G. Bruce, Angew. Chem. Int. Ed. 51 (2012) 9994–10024.
[3] J.N. Reimers, J.R. Dahn, J. Electrochem. Soc. 139 (1992) 2091–2097.
[4] G. Amatucci, J.M. Tarascon, J. Electrochem. Soc. 149 (2002) K31–K46.
[5] K. Amine, J. Liu, S. Kang, I. Belharouak, Y. Hyung, D. Vissers, G. Henriksen, J. Power Sources 129 (2004) 14–19.
[6] K.A. Walz, C.S. Johnson, J. Genthe, L.C. Stoiber, W.A. Zeltner, M.A. Anderson, M.M. Thackeray, J. Power Sources 195 (2010) 4943–4951.
[7] S.B. Park, H.C. Shin, W.G. Lee, W.I. Cho, H. Jang, J. Power Sources 180 (2008) 597–601.
[8] N. Yabuuchi, T. Ohzuku, J. Power Sources 119 (2003) 171–174.
[9] M.H. Lee, Y. Kang, S.T. Myung, Y.K. Sun, Electrochim. Acta 50 (2004) 939–948.
[10] Y.K. Sun, Z.H. Chen, H.J. Noh, D.J. Lee, H.G. Jung, Y. Ren, S. Wang, C.S. Yoon, S.T. Myung, K. Amine, Nat. Mater. 11 (2012) 942–947.
[11] E. Hosono, T. Kudo, I. Honma, H. Matsuda, H.S. Zhou, Nano Lett. 9 (2009) 1045–1051.
[12] H.W. Lee, P. Muralidharan, R. Ruffo, C.M. Mari, Y. Cui, D.K. Kim, Nano Lett. 10 (2010) 3852–3856.
[13] K.M. Shaju, P.G. Bruce, Chem. Mater. 20 (2008) 5557–5562.
[14] S.H. Kang, J.B. Goodenough, L.K. Rabenberg, Electrochem. Solid State Lett. 4 (2001) A49–A51.
[15] H.M. Wu, J.P. Tu, Y.F. Yuan, X.T. Chen, J.Y. Xiang, X.B. Zhao, G.S. Cao, J. Power Sources 161 (2006) 1260–1263.
[16] C.H. Jiang, S.X. Dou, H.K. Liu, M. Ichihara, H.S. Zhou, J. Power Sources 172 (2007) 410–415.
[17] B.J. Liddle, S.M. Collins, B.M. Bartlett, Energy Environ. Sci. 3 (2010) 1339–1346.
[18] M.J. Zhi, A. Manivannan, F.K. Meng, N.Q. Wu, J. Power Sources 208 (2012) 345–353.
[19] Y.S. Luo, J. Jiang, W.W. Zhou, H.P. Yang, J.S. Luo, X.Y. Qi, H. Zhang, D.Y.W. Yu, C.M. Li, T. Yu, J. Mater. Chem. 22 (2012) 8634–8640.
[20] H.J. Yue, X.K. Huang, D.P. Lv, Y. Yang, Electrochim. Acta 54 (2009) 5363–5367.
[21] J.F. von Bulow, H.L. Zhang, D.E. Morse, Adv. Energy Mater. 2 (2012) 309–315.
[22] H. Xia, K.R. Ragavendran, J.P. Xie, L. Lu, J. Power Sources 212 (2012) 28–34.
[23] J.L. Li, C. Daniel, D. Wood, J. Power Sources 196 (2011) 2452–2460.
[24] C. Daniel, JOM 60 (2008) 43–48.
[25] R. Moshtev, B. Johnson, J. Power Sources 91 (2000) 86–91.
[26] J.C. Lytle, J.M. Wallace, M.B. Sassin, A.J. Barrow, J.W. Long, J.L. Dysart, C.H. Renninger, M.P. Saunders, N.L. Brandell, D.R. Rolison, Energy Environ. Sci. 4 (2011) 1913–1925.
[27] M. Yao, K. Okuno, T. Iwaki, M. Kato, S. Tanase, K. Emura, T. Sakai, J. Power Sources 173 (2007) 545–549.
[28] C.G. Yang, D.W. Zhang, Y.B. Zhao, Y.H. Lu, L. Wang, J.B. Goodenough, J. Power Sources 196 (2011) 10673–10678.
[29] M. Yao, K. Okuno, T. Iwaki, T. Awazu, T. Sakai, J. Power Sources 195 (2010) 2077–2081.
[30] A.H. Whitehead, M. Schreiber, J. Electrochem. Soc. 152 (2005) A2105–A2113.
[31] A.K. Kercher, J.O. Kiggans, N.J. Dudney, J. Electrochem. Soc. 157 (2010) A1323–A1327.
[32] S.K. Martha, J.O. Kiggans, J. Nanda, N.J. Dudney, J. Electrochem. Soc. 158 (2011) A1060–A1066.
[33] L. Yang, S. Cheng, Y. Ding, X.B. Zhu, Z.L. Wang, M.L. Liu, Nano Lett. 12 (2012) 321–325.
[34] M.K. Song, S. Cheng, H.Y. Chen, W.T. Qin, K.W. Nam, S.C. Xu, X.Q. Yang, A. Bongiorno, J. Lee, J.M. Bai, T.A. Tyson, J. Cho, M.L. Liu, Nano Lett. 12 (2012) 3483–3490.
[35] B. Liu, J. Zhang, X.F. Wang, G. Chen, D. Chen, C.W. Zhou, G.Z. Shen, Nano Lett. 12 (2012) 3005–3011.
[36] Y.C. Chen, K. Xie, Y. Pan, C.M. Zheng, J. Power Sources 196 (2011) 6493–6497.
[37] S.K. Martha, N.J. Dudney, J.O. Kiggans, J. Nanda, J. Electrochem. Soc. 159 (2012) A1652–A1658.
[38] X.L. Jia, C.Z. Yan, Z. Chen, R.R. Wang, Q. Zhang, L. Guo, F. Wei, Y.F. Lu, Chem. Commun. 47 (2011) 9669–9671.
[39] L.J. Fu, H. Liu, C. Li, Y.P. Wu, E. Rahm, R. Holze, H.Q. Wu, Solid State Sci. 8 (2006) 113–128.
[40] H.X. Ji, L.L. Zhang, M.T. Pettes, H.F. Li, S.S. Chen, L. Shi, R. Piner, R.S. Ruoff, Nano Lett. 12 (2012) 2446–2451.